

Magnetic moment enhancement at the Fe(100)/Co(bcc) interface: a nanometer-scale investigation from electron energy loss spectra

R. Serra¹, L. Calmels^{1,a}, S. Andrieu², and V. Serin¹

¹ CEMES-CNRS, Université de Toulouse, 29 rue Jeanne Marvig, BP 94347, 31055 Toulouse Cedex 4, France

² LPM UMR 7556 CNRS-Nancy Université, BP 239, 54506 Vandœuvre, France

Received: 29 September 2010 / Received in final form: 7 December 2010 / Accepted: 10 February 2011
Published online: 7 June 2011 – © EDP Sciences

Abstract. The electronic structure and the magnetic moment of metallic iron are strongly modified near the Fe(100)/Co(*bcc*) interface. This effect has been evaluated from the iron $L_{2,3}$ energy loss near edge structure recorded for Fe/Co superlattices grown by molecular beam epitaxy with different periods. The interface-induced modification of the intensity ratio $I(L_3)/I(L_2)$ which has been measured by electron energy loss spectroscopy is in good agreement with the enhancement of the magnetic moment calculated from first principles. This shows that the intensity ratio can be used to obtain information on magnetic moments at a nanometer scale in a transmission electron microscope.

1 Introduction

The chemical bond and the electronic structure are modified near an interface, where the nature and the position of the first neighbour atoms change abruptly. When magnetic materials are involved, interface effects also affect the magnetic moments which can be enhanced or lowered, and the magnetic anisotropy which can be modified. Strained cobalt layers and Fe/Co superlattices grown on a (100) iron buffer crystallize in the body-centered cubic (*bcc*) structure when the cobalt layers are very thin [1–5]. The magnetic properties of these systems have been studied in details and different conclusions have been drawn for the spin and the orbital magnetic moments of an iron and a cobalt atom located at one of the Fe/Co interfaces: the spin magnetic moment of an interface cobalt atom does not strongly differ from the bulk value, while it is enhanced for an interface iron atom [6–14]. The orbital magnetic moment decreases at the interface for a cobalt atom, while it slightly increases for an iron atom [10–13]. These interface-induced modifications of the magnetic moments can be enhanced by roughness and formation of a thin alloy layer at the Fe/Co interfaces [15,16]. In this case, the magnetic moments become close to those of the bulk alloy with identical composition [14]. Fe/Co interfaces are finally responsible for a modification of the magnetic anisotropy, with an easy magnetic axis which switches from the (100) to the (110) direction when the thickness of the *bcc* cobalt layers increases in Fe/Co superlattices [4,9–11,13,14,17].

The aim of this paper is to describe a method that gives access to the modification of magnetic moments induced by interfaces in Fe/Co *bcc* superlattices. This method uses a transmission electron microscope (TEM), and is based on electron energy loss spectroscopy (EELS) performed with a nanometer probe size [18,19]. Several authors have investigated the magnetic structure of materials from EELS spectra. The most recent technique which has been proposed to reach this aim consists in measuring the energy loss magnetic chiral dichroism (EMCD) [20–22] analogous of the X-ray magnetic circular dichroism (XMCD) which is recorded in X-ray absorption spectroscopy [23,24]. EMCD should give access to the measurement of the magnetic moments if suitable sum rules are used [25,26]. This technique is nevertheless in its early age and still needs experimental improvement before to give trustable values for the magnetic moments. Several authors have measured the white line ratio (WLR) $I(L_3)/I(L_2)$ at the $L_{2,3}$ edge of 3d transition metals to investigate the magnetic structure of these atoms. It has for instance been shown that alloying effects reduce both the iron magnetic moment and $L_{2,3}$ edge intensity ratio in $\text{Fe}_x\text{Ge}_{1-x}$ [27] and $\text{Fe}_x\text{Y}_{1-x}$ [28] alloys. Kurata represented the iron WLR as a function of its magnetic moment, for a large number of Fe-based compounds and alloys and showed that this ratio increases more or less linearly with the magnetic moment [29]. Based on the theoretical results of Thole and van der Laan [30], Pease suggested that a universal curve can be used to represent the WLR as a function of the magnetic moment. He evaluated the numerical values of this curve and showed that

^a e-mail: calmels@cemes.fr

they coincide quite well with experimental data recorded at the $L_{2,3}$ edge of different 3d transition metals [31]. The Co WLR has recently been measured for very thin cobalt layers, but the thickness dependence of this ratio could not undoubtedly be attributed to changes in the magnetic moment, because the atomic structure of the layers switches from *bcc* to hexagonal compact (*hcp*) when the thickness increases [32].

Thole and van der Laan used atomic calculations to understand why the branching ratio $I(L_3)/[I(L_2)+I(L_3)]$ of 3d transition metals deviates from its statistical value. The factors which are responsible for this deviation are: the valence of the absorbing atom, the nature (high spin or low spin) of the initial state, the electrostatic interaction between the core hole and the valence electrons, the crystal field parameter, and the spin orbit coupling for the valence states [30,33,34].

Theoretical and experimental studies have all shown that the WLR of a 3d transition metal atom generally increases with its magnetic moment. However, a clear relation, or a sum rule, relating these two quantities has never been established, and the absolute value of the magnetic moment cannot be obtained directly from the ratio extracted from EELS spectra. In the present paper, we compare the iron $L_{2,3}$ intensity ratio measured in several Fe(100)/Co(*bcc*) superlattices with different periods. The crystal structure and the valence state of the Fe and Co atoms are similar for all these samples which only differ by the number of iron layers. We found that the averaged value of the Fe WLR is higher in the superlattices than in bulk Fe. We suggest to use the relative (compared to bulk) enhancement of the Fe WLR as an indicator of the modification of the Fe magnetic moment induced by the interfaces in the Fe/Co superlattices. We compare the variations of the WLR measured by EELS with those of the magnetic moment obtained from first principles calculations performed for perfect structures, and we conclude that the relative enhancement of these two quantities is comparable.

Our paper is organized as follows: in Section 2, we present our samples and their growth conditions. The TEM analysis of these samples is described in Section 3. The spin magnetic moments calculated from first principles are presented in Section 4 where we compare the interface-induced enhancement of the Fe magnetic moment and WLR. We discuss our results in Section 5 and finally conclude in Section 6.

2 Sample growth

Samples were grown by molecular beam epitaxy (MBE). The base pressure during depositions was equal to 3×10^{-11} hPa. Reflection high energy electron diffraction (RHEED) was performed in situ during the growth process to control the flatness of the superlattices. Auger electron spectroscopy (AES), X-ray photoelectron spectroscopy (XPS), and a scanning tunnelling microscope (STM) were used inside the chamber to check at the end of the growth process that the surface of the samples is

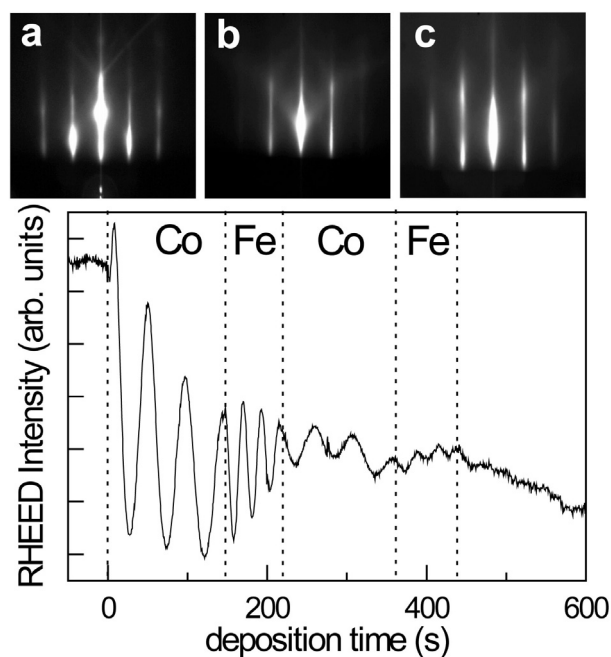


Fig. 1. Top: RHEED patterns along the [110] azimuth of the square MgO lattice for (a) the initial MgO substrate, (b) after the Fe buffer layer growth and (c) after the growth of a [Co(3MLs)/Fe(10MLs)] \times 20 superlattice. Bottom: RHEED intensity oscillations performed at room temperature during the growth of two Co(3MLs)/Fe(3MLs) bilayers, showing the layer by layer growth.

flat and free from any contamination. Fe and Co were sublimated by using Knudsen cells heated up respectively at 1520 K and 1720 K, leading to fluxes around 1 monolayer (ML) per minute. The Fe/Co superlattices were grown on a Fe buffer layer deposited on single-crystalline MgO substrates. To avoid any carbon contamination of the Fe buffer layer, a MgO buffer layer was grown first on the substrate [35]. The Fe buffer layer was thus grown at room temperature and heated up to 750 K to get a smooth surface with large terraces [36]. The superlattice stacking was

$$\text{Fe}(100 \text{ nm})/\text{Co}(3\text{MLs})/[\text{Fe}(n\text{MLs})/\text{Co}(3\text{MLs})]_p,$$

where p is the number of Fe/Co periods and n the number of monolayers in each Fe thin layer. This stacking is capped with a 2 nm thick MgO layer.

We have checked by AES that the Fe/Co interdiffusion occurs above 570 K. Consequently, the Fe and Co layers of the superlattices and the MgO cap layer were deposited at room temperature. Typical RHEED patterns observed during the process are shown in Figure 1. They illustrate the epitaxial growth and the very small roughness of the surface, even at the end of the stacking. The large RHEED intensity oscillations observed during the process attest that the stacking is grown layer by layer with flat and sharp interfaces. As an intensity oscillation corresponds to the completion of exactly 1 monolayer, this technique was used to control accurately the thicknesses of each Fe and Co layer in the superlattices. The amplitude of the RHEED oscillations decreases during the growth (Fig. 1).

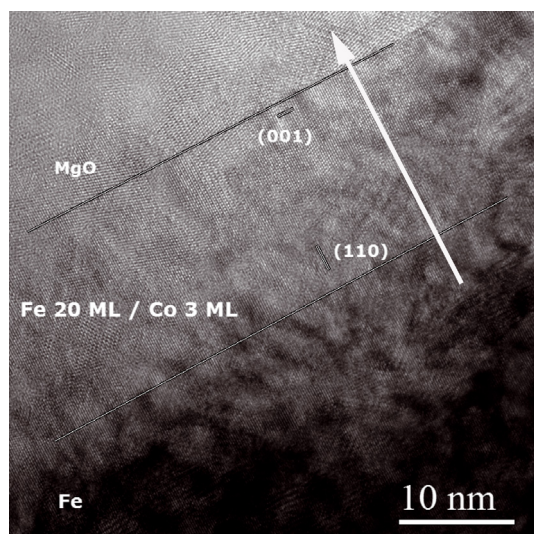


Fig. 2. HREM image obtained on the superlattice [Fe(20MLs)/Co(3MLs)] \times 5. The growth axis is represented by a white arrow. The figure shows the Fe buffer layer, the Fe/Co superlattice and the MgO cap layer. Interfaces are indicated by thin white lines.

This does not mean that roughness increases, but that the step density is higher, leading to smaller terraces and to a growth by step flow.

3 TEM analysis

Cross-section samples for TEM experiments were thinned using tripod polishing and ion-milling at low voltage to electron transparency. Samples were treated by plasma cleaner before any TEM observation. The TEM analysis was performed on a FEI Tecnai F20 operating at 200 kV and equipped with a field emission gun, an objective lens corrected for spherical aberration (CEOS), a scanning transmission electron microscope (STEM) stage and a GIF TRIDIEM filter. The samples were studied by TEM. Figure 2 displays a large area of one of the samples, including the Fe buffer, the superlattice and the MgO cap layer. Unfortunately, we did not observe a specific contrast related to the chemical and structural changes at the interfaces between cobalt and iron thin layers in the superlattice. These two metals have indeed nearly the same atomic number, and the distance between atomic layers is almost the same in *bcc* Fe and in *bcc* Co. This expected lack of contrast, together with the artifacts due to TEM preparation (thin surface oxide layer, non uniform thickness...), do not allow to visualize the sharpness of Fe/Co interfaces which has been indicated by RHEED.

EELS spectra were acquired with a dispersion of 0.2 eV/channel and over a 400 eV energy window which includes the O-K at 532 eV, the Fe- $L_{2,3}$, and the Co- $L_{2,3}$ edges at 708 eV and 779 eV, see Figure 3. The TEM-STEM analysis was performed with a probe size of 1.5 nm which gives information on the local electronic structure with a rather good signal-to-noise ratio. The associated

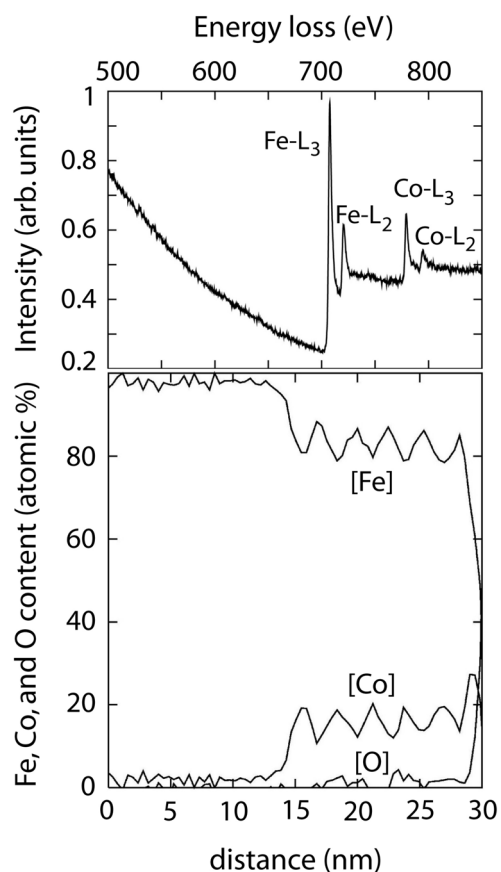


Fig. 3. Top: typical EELS spectrum measured on the [Fe(10MLs)/Co(3MLs)] \times 10 superlattice. The Fe and Co L_2 and L_3 edges are indicated. Bottom: EELS chemical profiles recorded along the white arrow drawn on the HREM image (Fig. 2), which reveals the chemical structure of the [Fe(20MLs)/Co(3MLs)] \times 5 superlattice.

pixel step and acquisition time were of 0.5 nm and 3 s. The sample spatial drift was automatically controlled and corrected during the STEM-EELS experiments using the Digital Micrograph acquisition software.

The local chemical composition along the growth axis of the samples (shown as a white arrow in Fig. 2) was measured by spatially resolved EELS as shown for the Fe(20MLs)/Co(3MLs) superlattice in the bottom part of Figure 3. The oscillations of the Fe and Co contents are clearly visible. The width of the probe (1.5 nm) used to measure the chemical profiles shown in Figure 3 is larger than the width of the thin Co layers. This is the reason why the curve which represents the Fe content does not vanish in the middle of the Co layers, while the curve which represents the Co content oscillates between 10 and 20 at.%. Oscillations in the chemical profiles could also be observed for the Fe(10MLs)/Co(3MLs) superlattice, but not for the samples in which the thickness of the Fe layers (5 and 3 MLs) is smaller than the spot size. We mention that the superlattices contain only metallic thin layers (the oxidation of the Fe and Co atoms was not observed in the spectra). A small concentration of oxygen atoms is gener-

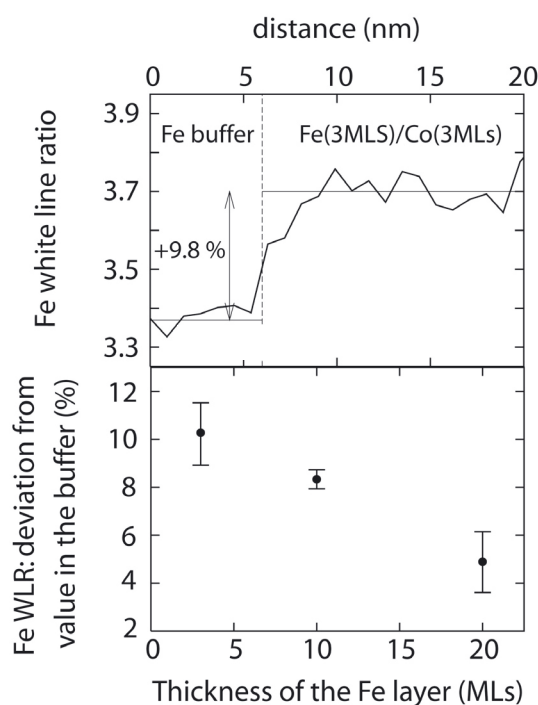


Fig. 4. Top: Fe white line ratio measured during one scan along the growth axis of the $[\text{Fe}(3\text{MLs})/\text{Co}(3\text{MLs})] \times 20$ superlattice. The accuracy of the measurements is $\pm 2.5\%$ of the WLR [39]. Bottom: relative enhancement (when compared to the Fe buffer) of the Fe white line ratio in the $\text{Fe}(n\text{MLs})/\text{Co}(3\text{MLs})$ superlattices, as a function of the number n of monolayers in the thin Fe layers of the superlattices. Each of these results corresponds to the value of the ratio averaged over several non overlapping scans. Error bars correspond to the standard deviation.

ally detected (see Fig. 3), and we assume that this is only due to a superficial contamination. This was confirmed by sputtering one of the superlattices up to the MgO substrate with Argon ions in ultra high vacuum (UHV), while recording the O and C Auger peaks: C and O atoms were not observed during this sputtering process. The intensity ratio $I(L_3)/I(L_2)$ was extracted from the energy second derivative of the EELS spectra, following the method proposed by Lytle [37] and by Botton [38]. The background of the spectra, which behaves like $I(E) \propto E^{-r}$, does not need to be subtracted with this method: $d^2I(E)/dE^2 \propto E^{-(r+2)}$ decreases very rapidly and does not contribute significantly to the second derivative of the spectra. The curve represented in the upper part of Figure 4 shows the spatial variation of the Fe WLR measured during one scan along the growth axis of the $\text{Fe}(3\text{MLs})/\text{Co}(3\text{MLs})$ superlattice. It shows that the WLR is nearly 10% higher in this superlattice than in the Fe buffer. A smaller but clear enhancement of this ratio can also be observed for the superlattices with larger periods. The relative enhancement (compared to the buffer layer) of the white line ratio is represented in the bottom part of Figure 4, as a function of the number of monolayers in the thin Fe layers of the superlattices. $I(L_3)/I(L_2)$ is found 4.9% higher in the $\text{Fe}(20\text{MLs})/\text{Co}(3\text{MLs})$ superlattice than in the Fe buffer.

The results shown in the bottom part of Figure 4 correspond to the value of the ratio averaged over several close (but non overlapping) scans parallel to the growth axis of the superlattices. The Co WLR takes approximately the same value (compared to the Fe ratio in the buffer) for all the superlattices, although the $\text{Co-}L_{2,3}$ near edge structure is difficult to measure.

4 Spin magnetic moments calculated from first principles and comparison with the measured white line ratio

We have calculated the Fe and Co spin magnetic moments in the perfect superlattices with the code Layer Korringa Kohn Rostoker (Layer-KKR). This multiple scattering code based on the local spin density approximation (LSDA) is well adapted to study the electronic structure of epitaxial systems which contain interfaces [40]. The lattice parameter which has been chosen for the calculations is that of bulk Fe (0.287 nm). This is justified in directions perpendicular to the growth axis because we are studying superlattices strained on a Fe buffer. This is also justified in the growth axis direction, because atomic layer relaxation is very small in $\text{Fe}(100)/\text{Co}$ multilayers, as mentioned in a recent study [13]. Our calculations use a muffin-tin radius of 0.141 nm for Fe and Co atoms, a maximum angular momentum $l_{\text{max}} = 4$, and a mesh of 36 Bloch wave vectors to perform integrations over the irreducible wedge of the first Brillouin zone.

The performed calculations show that the Fe spin magnetic moment mainly increases in the first Fe atomic layer at each interface, where the nature of the first neighbour atoms changes abruptly. This is a short range effect in the superlattices which contain a large number of Fe atomic layers: in these cases, the enhancement of the spin magnetic moment can mostly be observed in the first, second, third and fourth atomic layers where the magnetic moment is respectively 16%, 6%, 4%, and 2% higher than in bulk Fe. Consequently, the averaged Fe magnetic moment presented in Figure 5 is less affected by interface effects and decreases when the thickness of the Fe layers increases.

The enhancement of the measured Fe WLR in the superlattices is expected to be due to an increase of the Fe magnetic moment near the Fe/Co interfaces. Despite the non-perfect structure of the samples, see Figure 2, the measured Fe WLR and the calculated Fe averaged spin magnetic moment are both higher in the superlattices than in bulk Fe. The relative enhancement of these two quantities is comparable, as shown in Table 1. The Fe WLR is for instance approximately 10%, 8.3%, and 4.9% higher in the $\text{Fe}(3\text{MLs})/\text{Co}(3\text{MLs})$, the $\text{Fe}(10\text{MLs})/\text{Co}(3\text{MLs})$, and the $\text{Fe}(20\text{MLs})/\text{Co}(3\text{MLs})$ superlattices respectively than in the Fe buffer. The calculated averaged Fe spin magnetic moment is 13%, 5.0%, and 2.5% higher in the corresponding superlattices than in bulk Fe. The averaged value of the Fe spin magnetic moments increases in the same proportions than the Fe

Table 1. Comparison of the relative enhancement of the Fe white line ratio and calculated spin magnetic moment in the Fe(n MLs)/Co(3MLs) superlattices, as a function of the number n of monolayers in the thin Fe layers of the superlattices.

n	Enhancement of the Fe white line ratio	Enhancement of the Fe spin magnetic moment
3	+10.3%	+13.3%
10	+8.3%	+5.03%
20	+4.9%	+2.49%

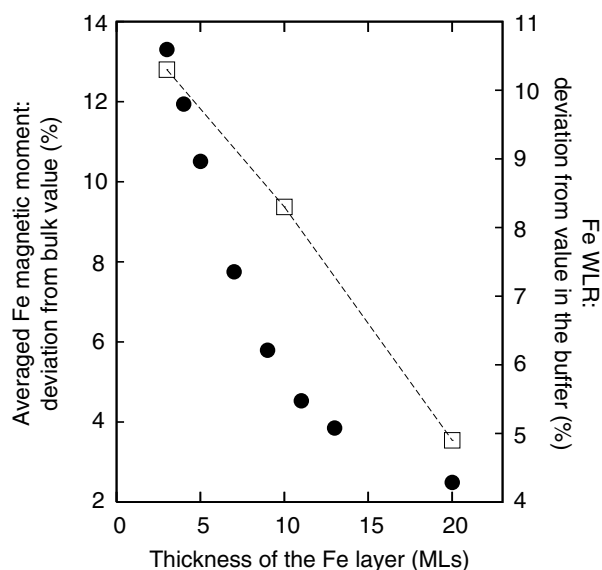


Fig. 5. (●) Relative enhancement (when compared to bulk Fe) of the Fe spin magnetic moment in the Fe(n MLs)/Co(3MLs) superlattices, calculated with the code Layer-KKR, as a function of the number n of monolayers in the thin Fe layers. (□) Relative enhancement (when compared to the Fe buffer) of the Fe WLR measured for several Fe(n MLs)/Co(3MLs) superlattices. The dashed line is a guide for the eyes.

WLR in the presence of Fe/Co interfaces. This is clearly visible in Figure 5.

5 Discussion

One of the limitations of the comparison between the measured WLR and the calculated averaged spin magnetic moment comes from the choice of the model which describes the atomic structure near the interfaces: our first principles calculation neglects for instance the fact that atomic steps cannot be fully avoided, as well as defects induced by the TEM preparation. These atomic steps and defects will modify the averaged Fe magnetic moment. Nevertheless, same trends are observed in experiments and calculations.

The enhancement of the Fe WLR in the superlattices can also be compared to the modification of the Fe orbital magnetic moment induced by the interfaces: Bergman et al. have shown that this moment is enhanced near the Fe/Co interfaces and that the averaged Fe orbital moment

of thin Fe layers containing 2, 4, and 6 MLs is respectively 12.8%, 8.2%, and 7.2% higher than that of bulk Fe [13]. This indicates that the averaged value of the Fe spin and orbital magnetic moments increase in the same proportions in the presence of Fe/Co interfaces.

Our results have shown a good correlation between the spin magnetic moment and the white line ratio of Fe atoms in metallic layers. This correlation would probably not have been observed for systems with nearly filled 3d bands such as Ni metal, for which a small spin orbit splitting of the valence bands can result in a significant enhancement of the WLR [31].

6 Conclusion

The combination of a STEM-EELS analysis of several Fe(100)/Co(*bcc*) superlattices with a first principles calculation of the magnetic moments has been used to show that the white line ratio recorded at the Fe- $L_{2,3}$ edge and the calculated averaged Fe magnetic moment increase in comparable proportions, compared to the bulk Fe values, when the superlattice period and the ratio of bulk to interface Fe atoms decrease. This comparison shows that the white line ratio can be very useful to obtain the local relative modification of the Fe magnetic moment induced by interfaces.

The calculations presented in this article have been performed at the CALMIP/UPS Toulouse parallel computer center. The authors would like to thank the IP3 project of the Sixth Framework Program of the European Commission: Enabling Science and Technology for European Electron Microscopy (ESTEEM) Contract No. 0260019 for funding.

References

1. P. Houdy, P. Boher, F. Giron, F. Pierre, C. Chappert, P. Beauvillain, K.L. Lang, P. Veillet, E. Velu, *J. Appl. Phys.* **69**, 5667 (1991)
2. J. Dekoster, E. Jedryka, C. Meny, G. Langouche, *J. Magn. Magn. Mater.* **121**, 69 (1993)
3. J. Dekoster, E. Jedryka, M. Wojcik, G. Langouche, *J. Magn. Magn. Mater.* **126**, 12 (1993)
4. P. Blomqvist, R. Wäppling, A. Broddefalk, P. Nordblad, S.G.E. te Velthuis, G.P. Felcher, *J. Magn. Magn. Mater.* **248**, 75 (2002)
5. P. Blomqvist, R. Wäppling, *J. Cryst. Growth* **252**, 120 (2003)
6. A.M.N. Niklasson, B. Johansson, H.L. Skriver, *Phys. Rev. B* **59**, 6373 (1999)
7. B. Kalska, P. Blomqvist, L. Häggström, R. Wäppling, *J. Phys.: Condens. Matter* **13**, 2963 (2001)
8. B. Kalska, P. Blomqvist, L. Häggström, R. Wäppling, *J. Magn. Magn. Mater.* **226–230**, 1773 (2001)
9. L. Häggström, B. Kalska, E. Nordström, P. Blomqvist, R. Wäppling, *J. Alloys Compd.* **347**, 252 (2002)
10. O. Eriksson, L. Bergqvist, E. Holmström, A. Bergman, O. LeBacq, S. Frota-Pessôa, B. Hjökvarsson, L. Nordsrom, *J. Phys.: Condens. Matter* **15**, S599 (2003)

11. M. Björck, G. Andersson, B. Lindgren, R. Wäppling, V. Stanciu, P. Nordblad, J. Magn. Magn. Mater. **284**, 273 (2004)
12. A. Bergman, E. Holmström, A.M.N. Niklasson, L. Nordström, S. Frota-Pessôa, O. Eriksson, Phys. Rev. B **70**, 174446 (2004)
13. A. Bergman, T. Burkert, B. Sanyal, S. Frota-Pessôa, L. Nordström, A.V. Ruban, S.I. Simak, O. Eriksson, Phys. Rev. B **74**, 174409 (2006)
14. S. Kamali, A. Bergman, G. Andersson, V. Stanciu, L. Häggström, J. Phys.: Condens. Matter **18**, 5807 (2006)
15. J. Dekoster, H. Bemelmans, S. Degroote, J. deWachter, E. Jedryka, R. Moons, A. Vantomme, G. Langouche, Hyperfine Interact. **95**, 191 (1995)
16. P. Panissod, J.P. Jay, C. Men y, M. Wojcik, E. Jedryka, Hyperfine Interact. **97-98**, 75 (1996)
17. B. Swinnen, J. Dekoster, G. Langouche, M. Rots, J. Magn. Magn. Mater. **148**, 148 (1995)
18. P.E. Batson, Nature **366**, 727 (1993)
19. D.A. Muller, T. Sorsch, S. Moccio, F.H. Baumann, K. Evans-Lutterodt, G. Timp, Nature **399**, 758 (1999)
20. C. Hébert, P. Schattschneider, Ultramicroscopy **96**, 463 (2003)
21. P. Schattschneider, S. Rubino, C. Hébert, J. Ruzs, J. Kunes, P. Novák, E. Carlino, M. Fabrizioli, G. Panaccione, G. Rossi, Nature **441**, 486 (2006)
22. B. Warot-Fonrose, F. Houdellier, M.J. Hytch, L. Calmels, V. Serin, E. Snoeck, Ultramicroscopy **108**, 393 (2008)
23. G. Schutz, W. Wagner, W. Wilhelm, P. Kienle, R. Zeller, R. Frahm, G. Materlik, Phys. Rev. Lett. **58**, 737 (1987)
24. C.T. Chen, Y.U. Idzerda, H.J. Lin, N.V. Smith, G. Meigs, E. Chaban, G.H. Ho, E. Pellegrin, F. Sette, Phys. Rev. Lett. **75**, 152 (1995)
25. L. Calmels, F. Houdellier, B. Warot-Fonrose, C. Gatel, M.J. Hytch, V. Serin, E. Snoeck, P. Schattschneider, Phys. Rev. B **76**, 060409(R) (2007)
26. J. Ruzs, O. Eriksson, P. Novák, P.M. Oppeneer, Phys. Rev. B **76**, 060408(R) (2007)
27. T.I. Morrison, M.B. Brodsky, N.J. Zaluzec, L.R. Sill, Phys. Rev. B **32**, 3107 (1985)
28. T.I. Morrison, C.L. Foiles, D.M. Pease, N.J. Zaluzec, Phys. Rev. B **36**, 3739 (1987)
29. H. Kurata, N. Tanaka, Microsc. Microanal. Microstruct. **2**, 183 (1991)
30. B.T. Thole, G. van der Laan, Phys. Rev. B **38**, 3158 (1988)
31. D.M. Pease, A. Fasihuddin, M. Daniel, J.I. Budnick, Ultramicroscopy **88**, 1 (2001)
32. B. Warot-Fonrose, A. Traverse, L. Calmels, V. Serin, E. Snoeck, Micron **37**, 478 (2006)
33. B.T. Thole, G. van der Laan, Phys. Rev. A **38**, 1943 (1988)
34. G. van der Laan, B.T. Thole, Phys. Rev. Lett. **60**, 1977 (1988)
35. M. Sicot, S. Andrieu, C. Tiusan, F. Bertran, F. Montaigne, J. Appl. Phys. **99**, 301 (2006)
36. M. Sicot, S. Andrieu, P. Turban, Y. Fagot-Revurat, H. Cercellier, A. Tagliaferri, C. De Nadai, N.B. Brookes, F. Bertran, F. Fortuna, Phys. Rev. B **68**, 184406 (2003)
37. F.W. Lytle, R.G. Greigor, Appl. Phys. Lett. **56**, 192 (1990)
38. G.A. Botton, C.C. Appel, A. Horsewell, W.M. Stobbs, J. Microsc. **180**, 211 (1995)
39. R. Serra, Ph.D. thesis, Université de Toulouse, 2009, http://thesesups.ups-tlse.fr/607/1/Serra_Raphael.pdf
40. J.M. MacLaren, S. Crampin, D.D. Vvedensky, J.B. Pendry, Phys. Rev. B **40**, 12164 (1989)